SUPPLEMENTARY INFORMATION

(1,2-azole)bis(bipyridyl)ruthenium(II) complexes: electrochemistry, luminescent properties, and electro- and photocatalysts for CO_2 reduction

Elena Cuéllar,[a] Laura Pastor,[a] Gabriel García-Herbosa,[b] John Nganga,[c] Alfredo M. Angeles-Boza,[c] Alberto Diez-Varga,[b] Tomás Torroba,[b] Jose M. Martín-Alvarez,[a] Daniel Miguel,[a] and Fernando Villafañe[a]*

[a] GIR MIOMeT-IU Cinquima-Química Inorgánica, Facultad de Ciencias, Campus Miguel Delibes, Universidad de Valladolid, 47011 Valladolid, Spain.

[b] Departamento de Química, Facultad de Ciencias, Universidad de Burgos, 09001 Burgos, Spain.

[c] Department of Chemistry, University of Connecticut, 55 N. Eagleville Rd, Storrs, CT 06269, USA.

Index

1. Cyclic voltammograms

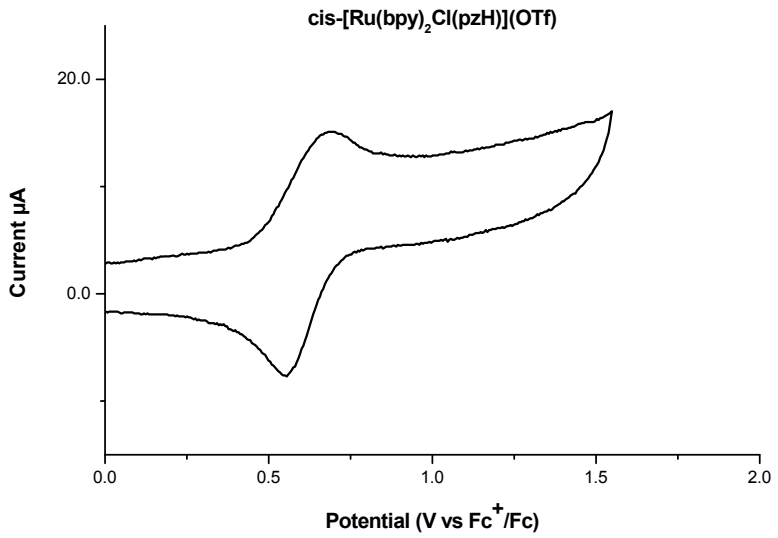

Figure S1. Cyclic voltammogram of 0.5mM cis-[Ru(bpy)$_2$Cl(pzH)](OTf) (1a) (glassy carbon working electrode dish 3.0 mm diameter, dry acetonitrile, 0.1 M Bu_4NPF_6) bubbling Ar to the sample, scan rate: 100 mVs^{-1}.

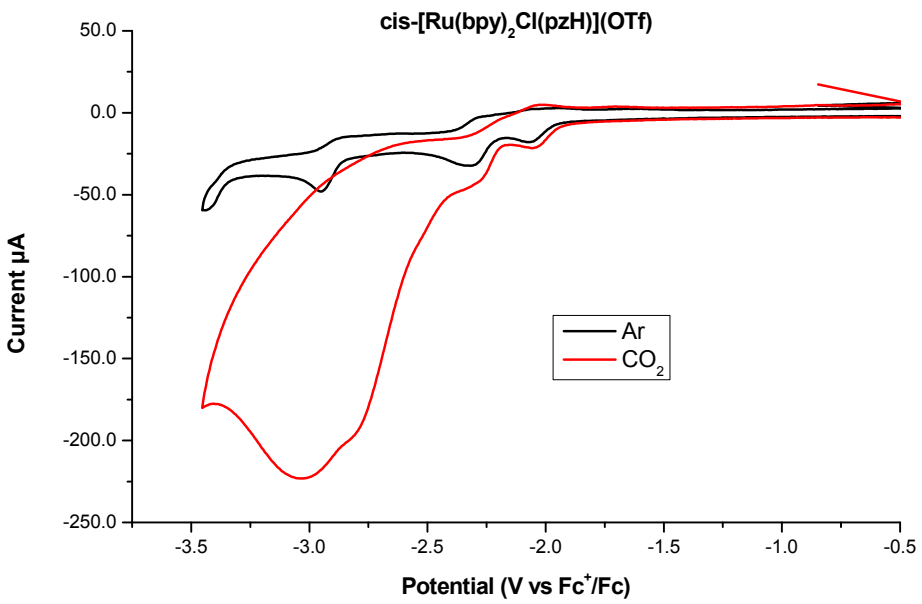

Figure S2. Cyclic voltammograms of 0.5mM cis-[Ru(bpy)$_2$Cl(pzH)](OTf) (1a) (glassy carbon working electrode dish 3.0 mm diameter, dry acetonitrile, 0.1 M Bu_4NPF_6) under Ar (black), and after bubbling CO_2 (red).

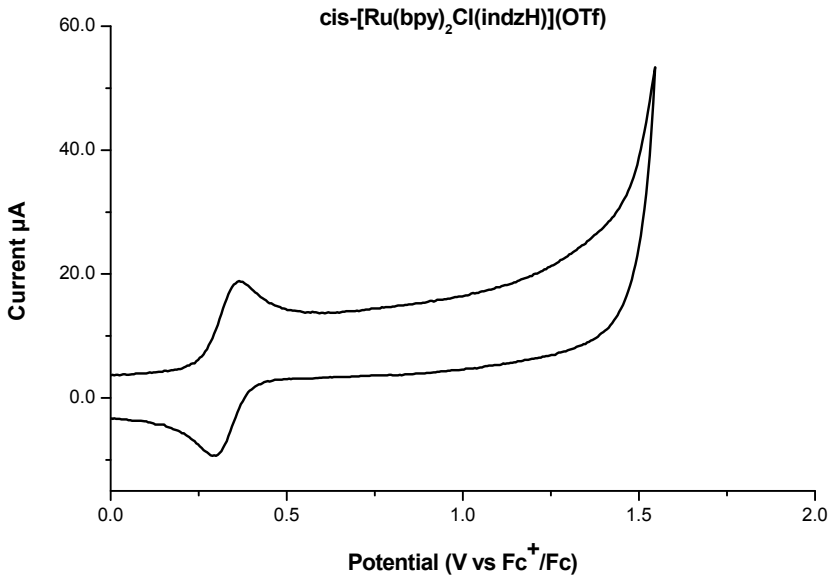

Figure S3. Cyclic voltammogram of 0.5mM cis-[Ru(bpy)$_2$Cl(indzH)](OTf) (1b) (glassy carbon working electrode dish 3.0 mm diameter, dry acetonitrile, 0.1 M Bu_4NPF_6) bubbling Ar to the sample, scan rate: 100 mVs^{-1}.

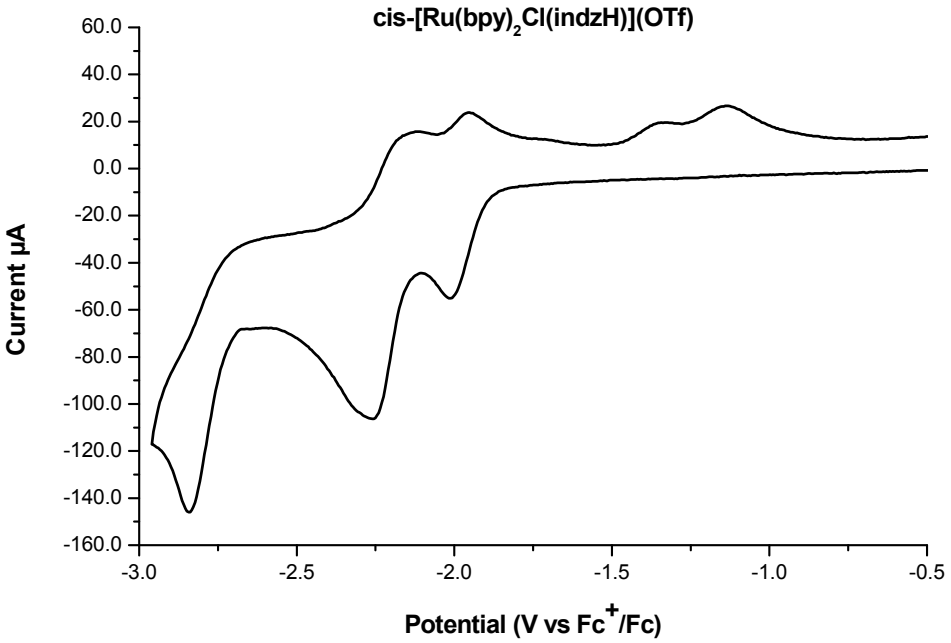

Figure S4. Cyclic voltammogram of 0.5mM cis-[Ru(bpy)$_2$Cl(indzH)](OTf) (1b) (glassy carbon working electrode dish 3.0 mm diameter, dry acetonitrile, 0.1 M Bu_4NPF_6) bubbling Ar to the sample, scan rate: 500 mVs^{-1}.

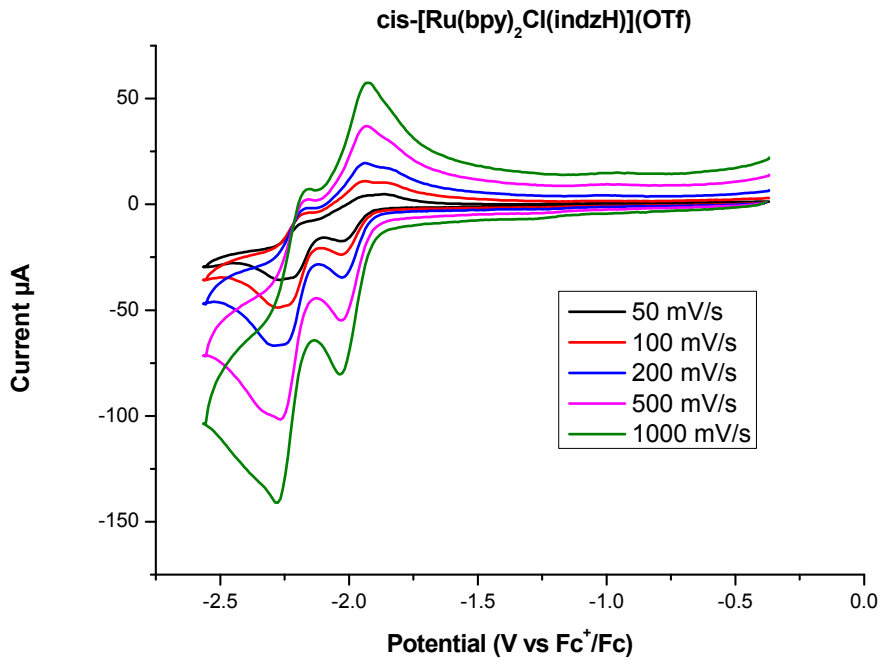

Figure S5. Cyclic voltammograms of 0.5mM cis-[Ru(bpy)$_2$Cl(indzH)](OTf) (1b) (glassy carbon working electrode dish 3.0 mm diameter, dry acetonitrile, 0.1 M Bu_4NPF_6) bubbling Ar to the sample, at different scan rates.

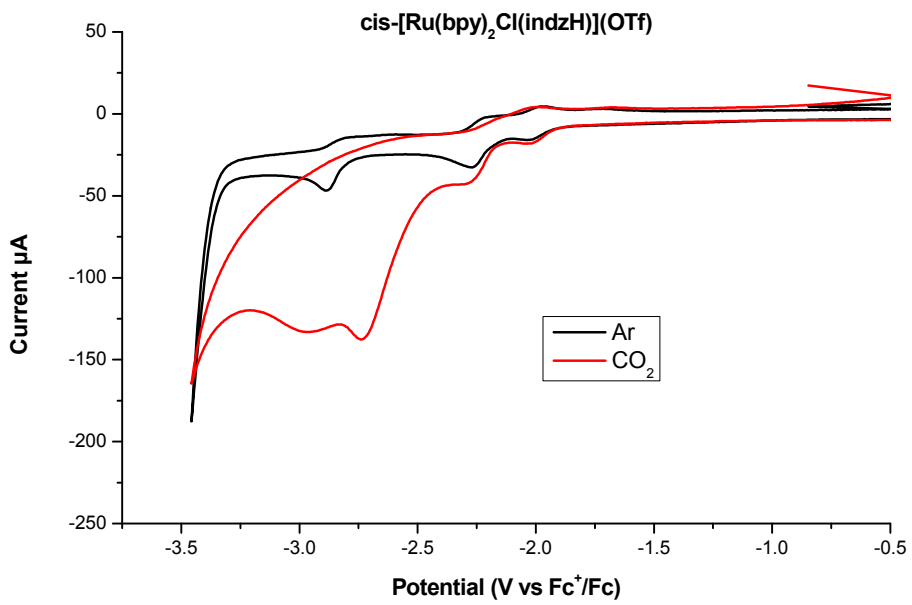

Figure S6. Cyclic voltammograms of 0.5mM cis-[Ru(bpy)$_2$Cl(indzH)](OTf) (1b) (glassy carbon working electrode dish 3.0 mm diameter, dry acetonitrile, 0.1 M Bu_4NPF_6) under Ar (black), and after bubbling CO_2 (red).

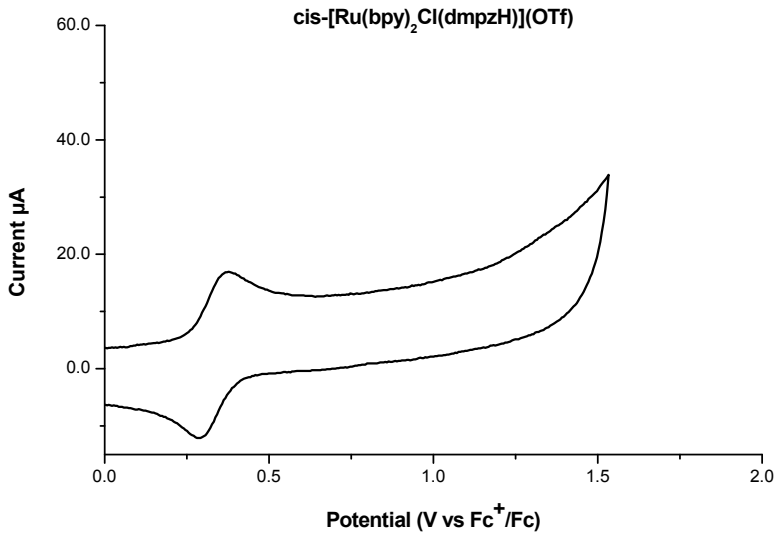

Figure S7. Cyclic voltammogram of 0.5mM cis-[Ru(bpy)$_2$Cl(dmpzH)](OTf) (1c) (glassy carbon working electrode dish 3.0 mm diameter, dry acetonitrile, 0.1 M Bu_4NPF_6) bubbling Ar to the sample, scan rate: 100 mVs^{-1}.

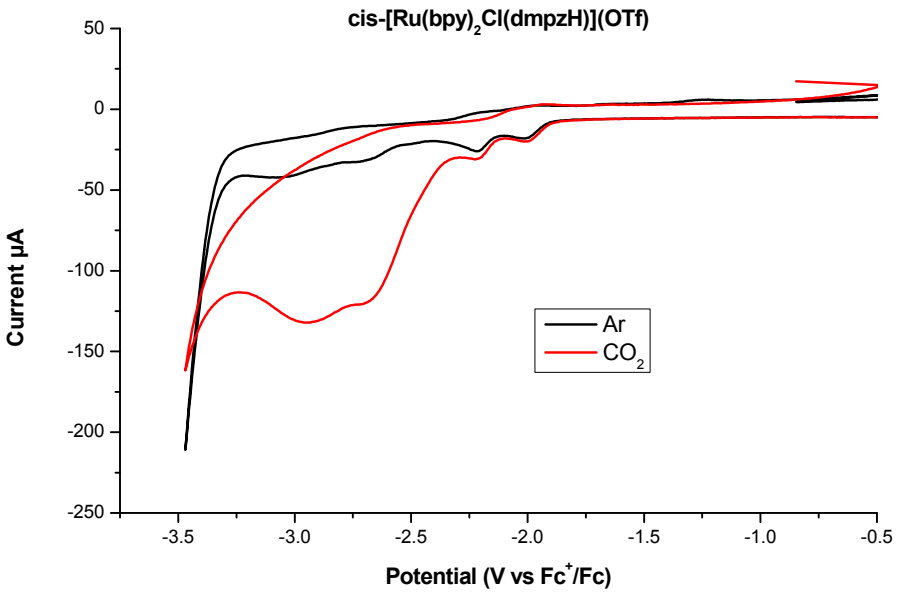

Figure S8. Cyclic voltammograms of 0.5mM cis-[Ru(bpy)$_2$Cl(dmpzH)](OTf) (1c) (glassy carbon working electrode dish 3.0 mm diameter, dry acetonitrile, 0.1 M Bu_4NPF_6) under Ar (black), and after bubbling CO_2 (red).

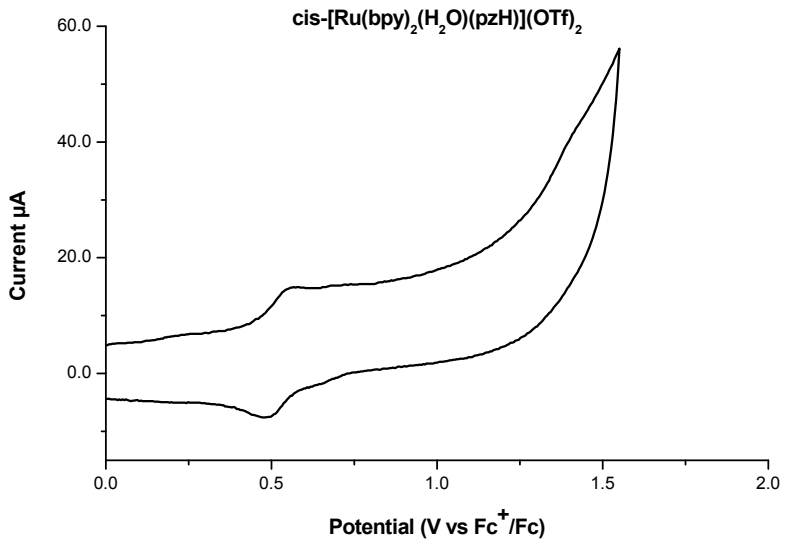

Figure S9. Cyclic voltammogram of 0.5mM cis-[Ru(bpy)$_2$(H$_2$O)(pzH)](OTf)$_2$ (2a) (glassy carbon working electrode dish 3.0 mm diameter, dry acetonitrile, 0.1 M Bu_4NPF_6) bubbling Ar to the sample, scan rate: 100 mVs^{-1}.

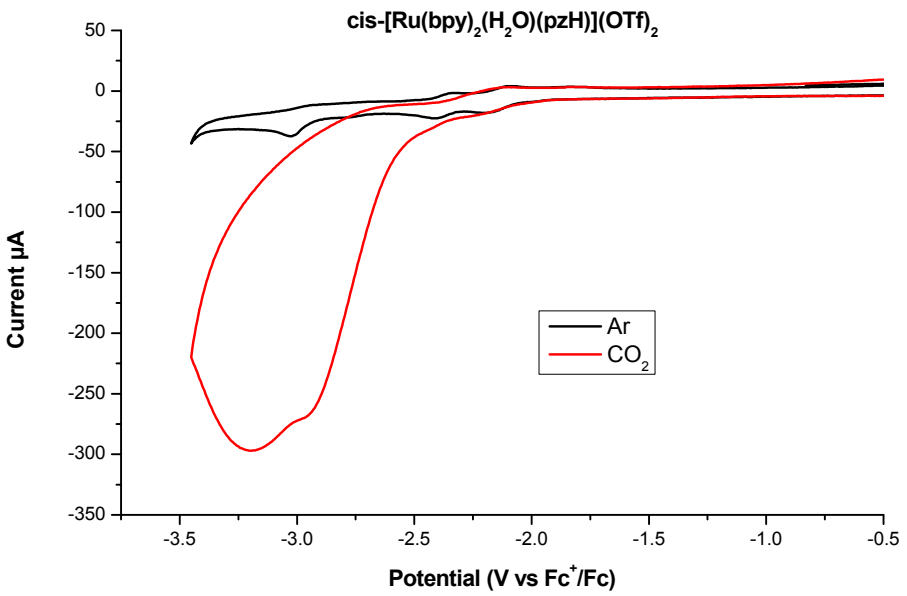

Figure S10. Cyclic voltammograms of 0.5mM cis-[Ru(bpy)2(H$_2$O)(pzH)](OTf)$_2$ (2a) (glassy carbon working electrode dish 3.0 mm diameter, dry acetonitrile, 0.1 M Bu_4NPF_6) under Ar (black), and after bubbling CO_2 (red).

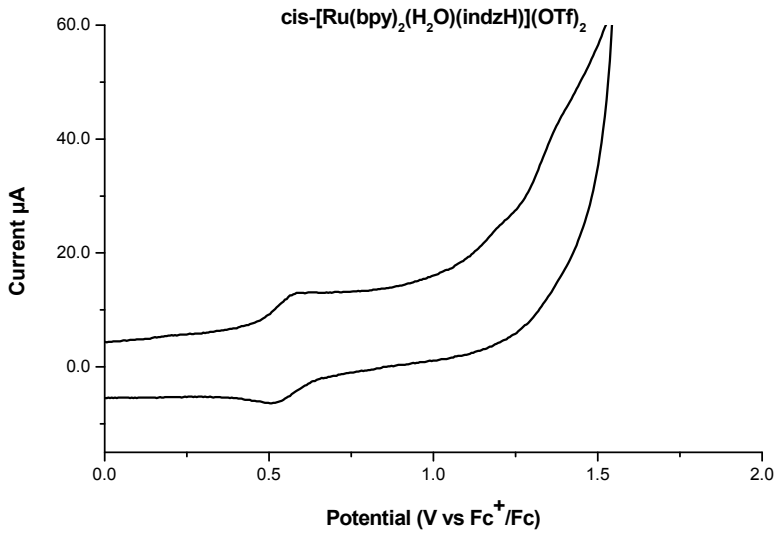

Figure S11. Cyclic voltammogram of 0.5mM cis-[Ru(bpy)2(H_2O)(indzH)]($OTf)_2$ (2b) (glassy carbon working electrode dish 3.0 mm diameter, dry acetonitrile, 0.1 M Bu_4NPF_6) bubbling Ar to the sample, scan rate: 100 mVs^{-1}.

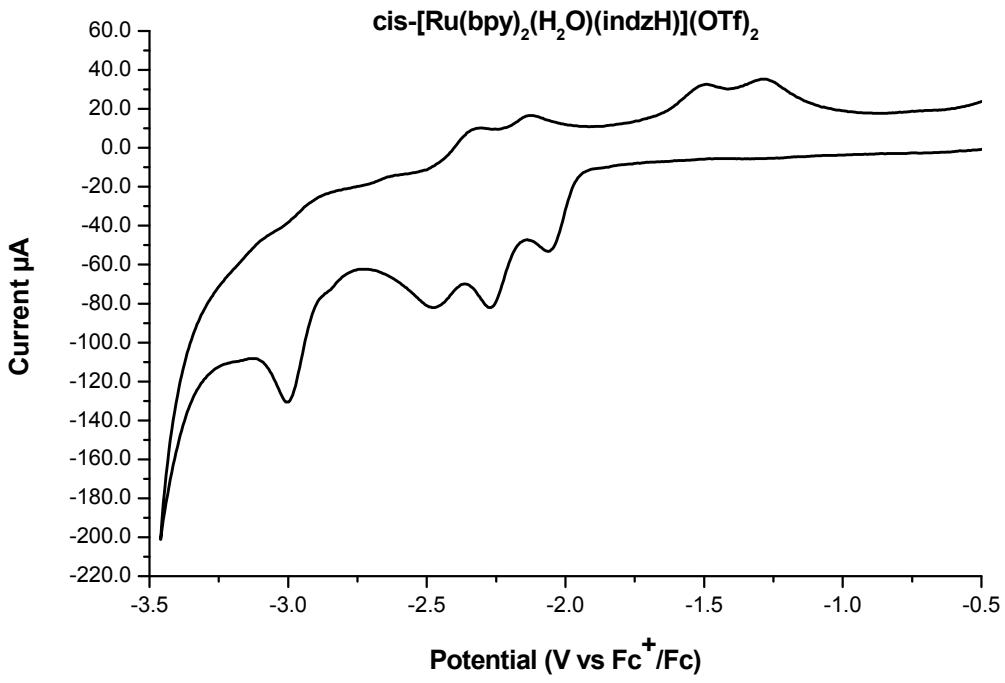

Figure S12. Cyclic voltammogram of 0.5mM cis-[Ru(bpy)2(H_2O)(indzH)]($OTf)_2$ (2b) (glassy carbon working electrode dish 3.0 mm diameter, dry acetonitrile, 0.1 M Bu_4NPF_6) bubbling Ar to the sample, scan rate: 500 mVs^{-1}.

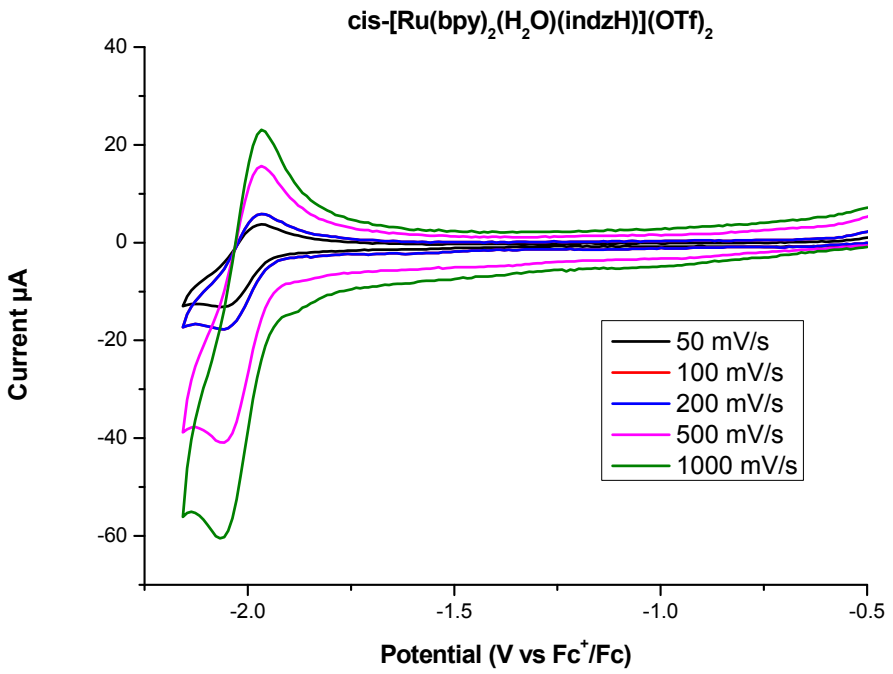

Figure S13. Cyclic voltammograms of 0.5mM cis-[Ru(bpy)2(H_2O)(indzH)](OTf)$_2$ (2b) (glassy carbon working electrode dish 3.0 mm diameter, dry acetonitrile, 0.1 M Bu_4NPF_6) bubbling Ar to the sample, at different scan rates.

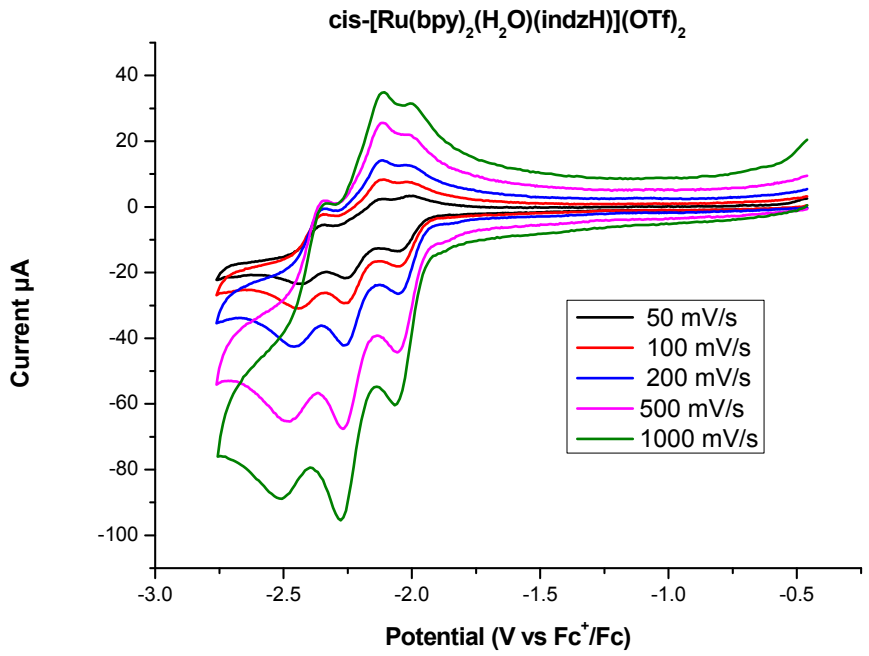

Figure S14. Cyclic voltammograms of 0.5mM cis-[Ru(bpy)2(H_2O)(indzH)](OTf)$_2$ (2b) (glassy carbon working electrode dish 3.0 mm diameter, dry acetonitrile, 0.1 M Bu_4NPF_6) bubbling Ar to the sample, at different scan rates.

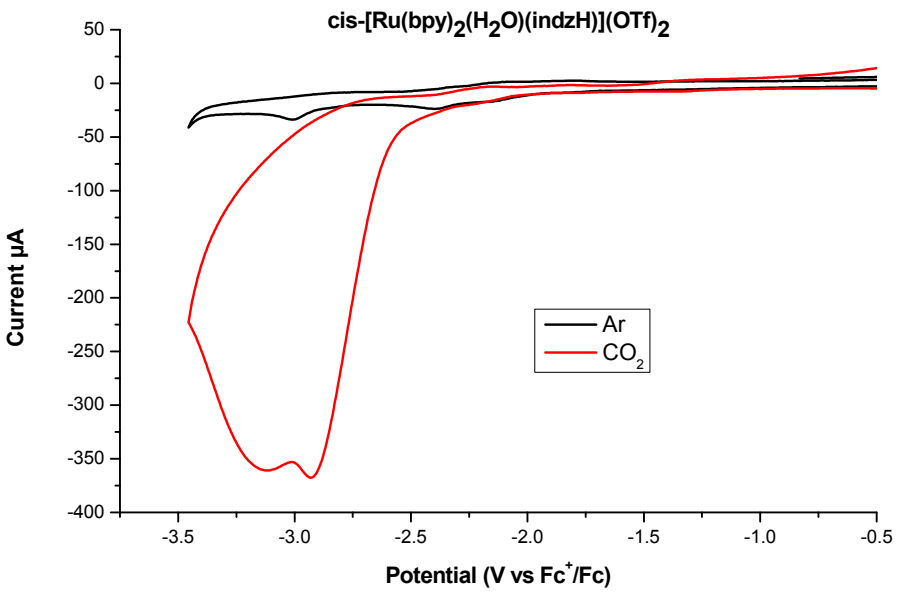

Figure S15. Cyclic voltammograms of 0.5mM cis-[Ru(bpy)$_2$(H$_2$O)(indzH)](OTf)$_2$ (2b) (glassy carbon working electrode dish 3.0 mm diameter, dry acetonitrile, 0.1 M Bu_4NPF_6) under Ar (black), and after bubbling CO_2 (red).

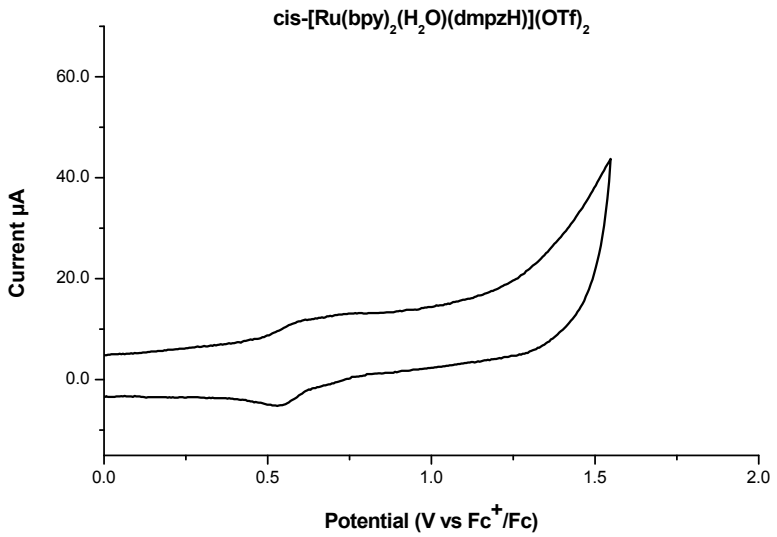

Figure S16. Cyclic voltammogram of 0.5mM cis-[Ru(bpy)$_2$(H$_2$O)(dmpzH)](OTf)$_2$ (2c) (glassy carbon working electrode dish 3.0 mm diameter, dry acetonitrile, 0.1 M Bu_4NPF_6) bubbling Ar to the sample, scan rate: 100 mVs^{-1}.

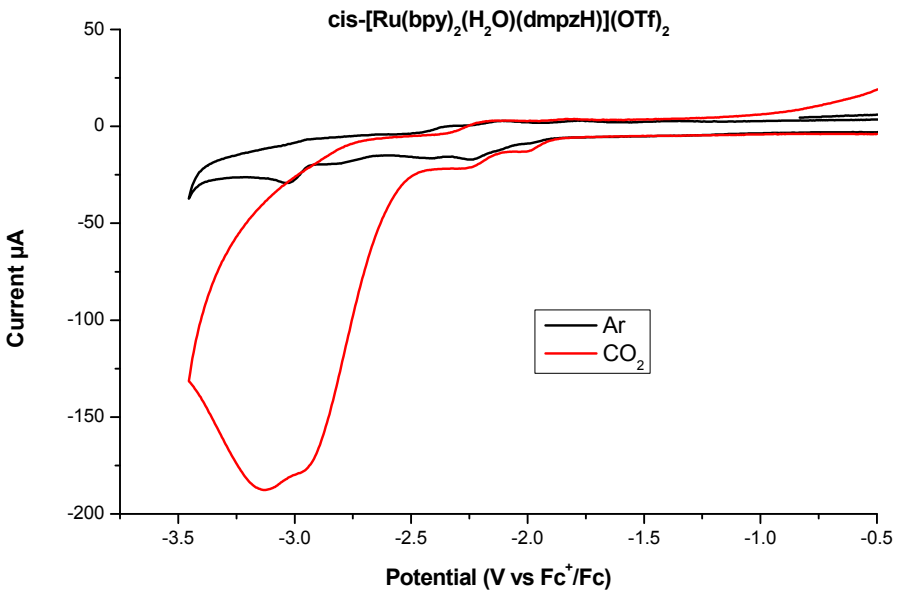

Figure S17. Cyclic voltammograms of 0.5mM cis-[Ru(bpy)$_2$(H$_2$O)(dmpzH)](OTf)$_2$ (2c) (glassy carbon working electrode dish 3.0 mm diameter, dry acetonitrile, 0.1 M Bu_4NPF_6) under Ar (black), and after bubbling CO_2 (red).

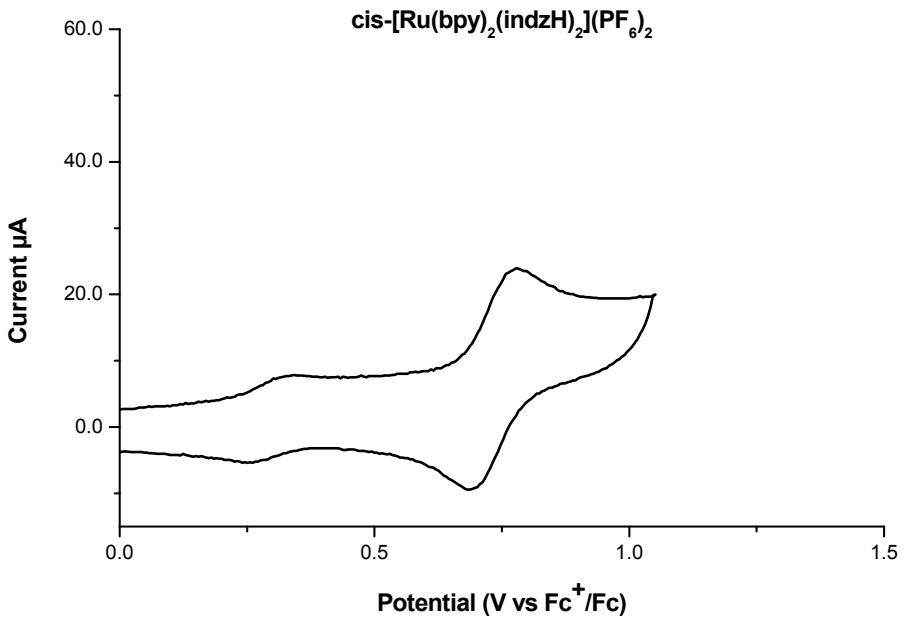

Figure S18. Cyclic voltammogram of 0.5mM cis-[Ru(bpy)$_2$(indzH)$_2$](PF$_6$)$_2$ (3) (glassy carbon working electrode dish 3.0 mm diameter, dry acetonitrile, 0.1 M Bu_4NPF_6) bubbling Ar to the sample, scan rate: 100 mVs^{-1}.

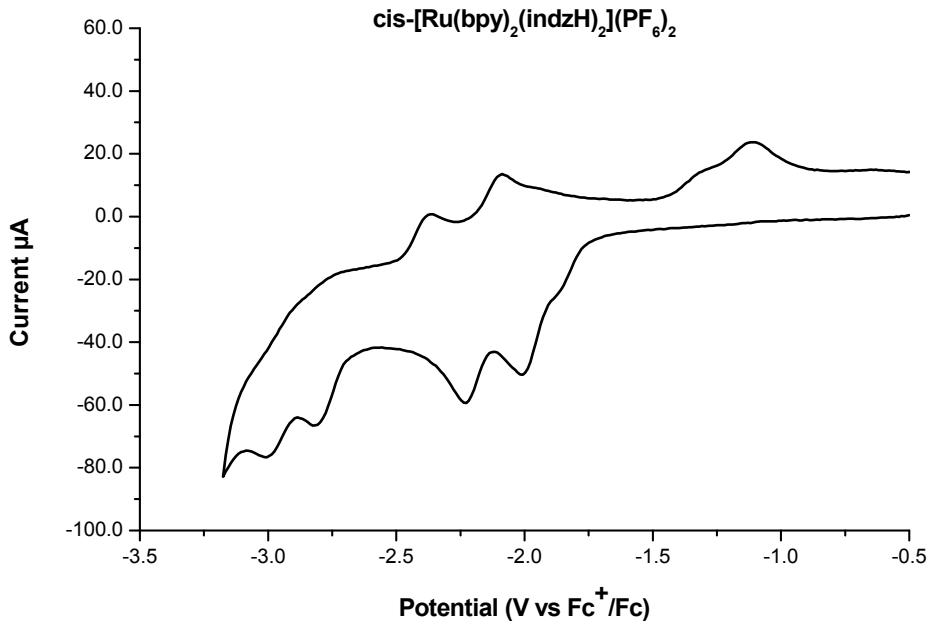

Figure S19. Cyclic voltammogram of 0.5mM cis-[Ru(bpy)$_2$(indzH)$_2$](PF$_6$)$_2$ (3) (glassy carbon working electrode dish 3.0 mm diameter, dry acetonitrile, 0.1 M Bu_4NPF_6) bubbling Ar to the sample, scan rate: 500 mVs^{-1}.

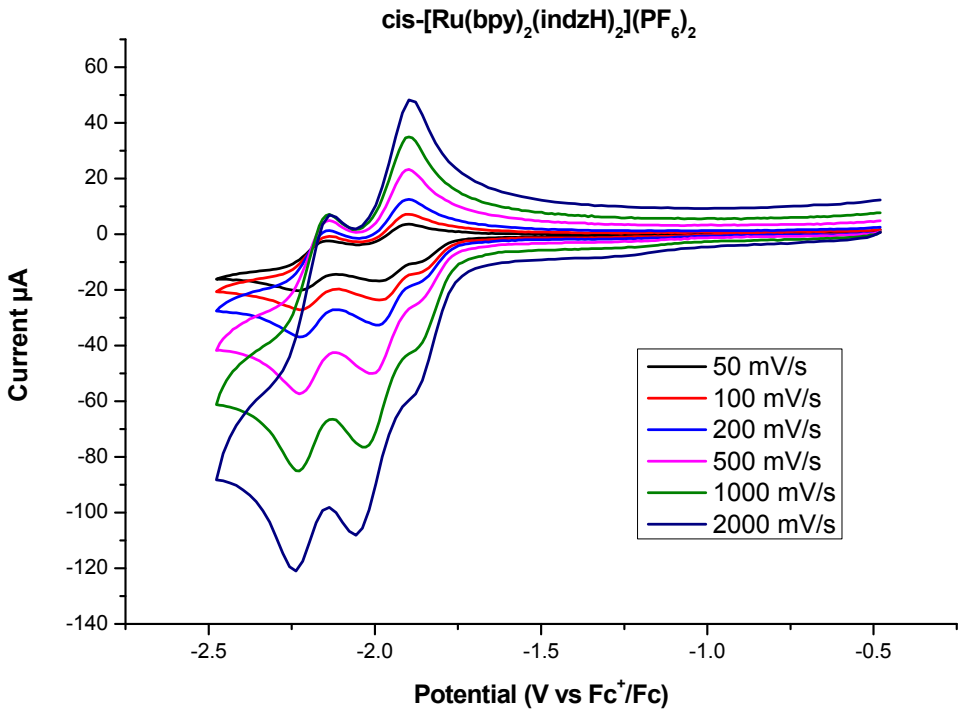

Figure S20. Cyclic voltammograms of 0.5mM cis-[Ru(bpy)$_2$(indzH)$_2$](PF$_6$)$_2$ (3) (glassy carbon working electrode dish 3.0 mm diameter, dry acetonitrile, 0.1 M Bu_4NPF_6) bubbling Ar to the sample, at different scan rates.

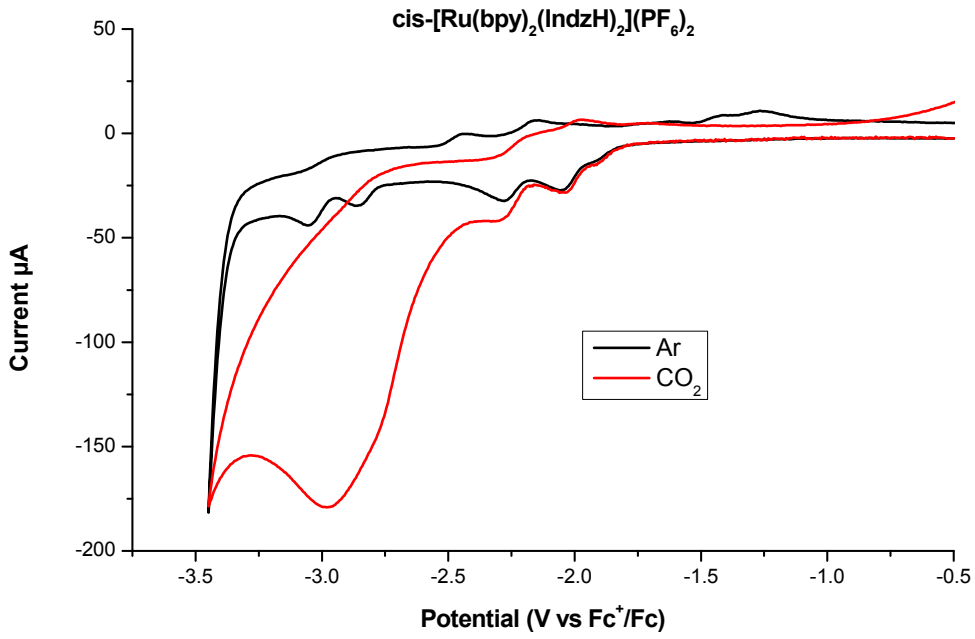

Figure S21. Cyclic voltammograms of 0.5mM cis-[Ru(bpy)$_2$(IndzH)$_2$](PF$_6$)$_2$ (3) (glassy carbon working electrode dish 3.0 mm diameter, dry acetonitrile, 0.1 M Bu_4NPF_6) under Ar (black), and after bubbling CO_2 (red).

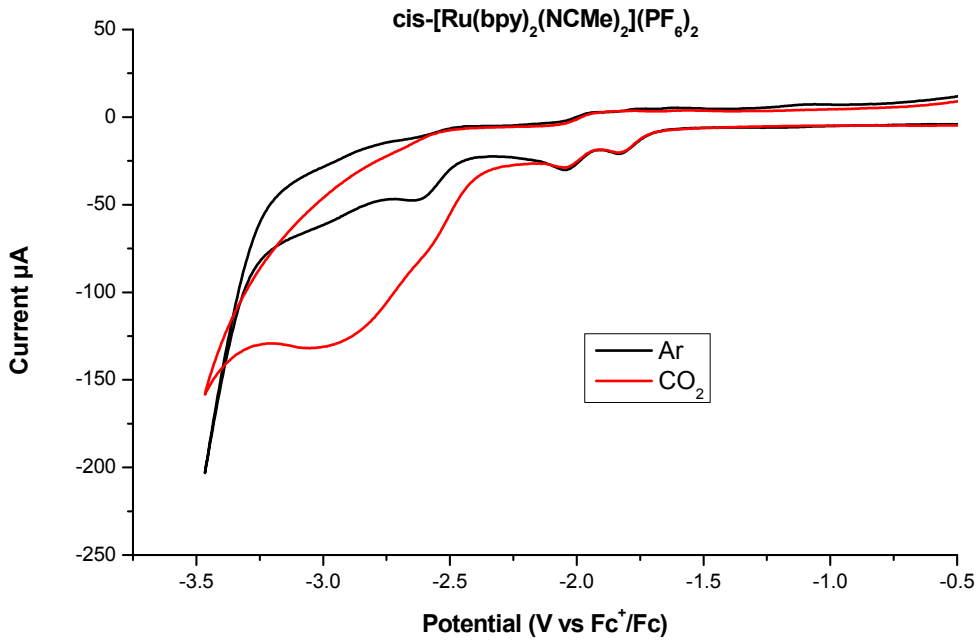

Figure S22. Cyclic voltammograms of 0.5mM cis-[Ru(bpy)$_2$(NCMe)$_2$](PF$_6$)$_2$ (4) (glassy carbon working electrode dish 3.0 mm diameter, dry acetonitrile, 0.1 M Bu_4NPF_6) under Ar (black), and after bubbling CO_2 (red).

2. Luminescence

1a:

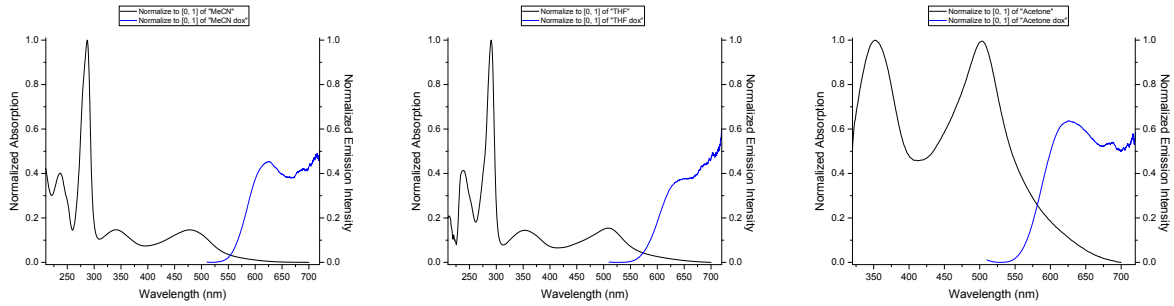

1a	**Absorption** λ nm (ε x 10^{-3} $M^{-1}cm^{-1}$)	**Emission** λ nm (% decrease)
MeCN	237 (19871), 287 (49483), 341 (7277), 477 (7263)	625 (34%)
THF	239 (24819), 291 (59853), 354 (8751), 508 (9339)	648 (64%)
Acetone	353 (8379), 504 (8341)	629 (63%)

1b:

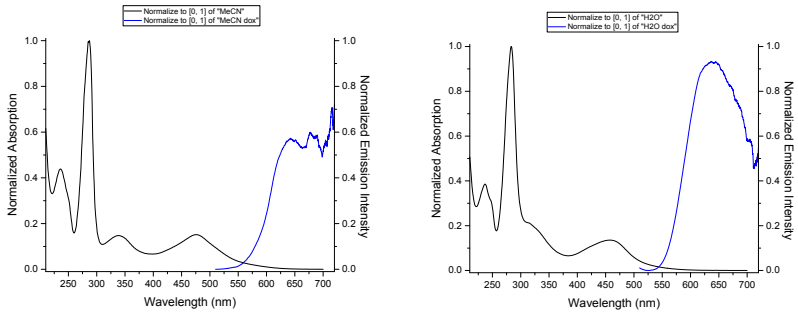

1b	**Absorption** λ nm (ε x 10^{-3} $M^{-1}cm^{-1}$)	**Emission** λ nm (% decrease)
MeCN	236 (24093), 287 (54918), 338 (8109), 476 (8328)	646 (37%)
H_2O	237 (18771), 284 (48675), 458 (6598)	629 (2%)

1c:

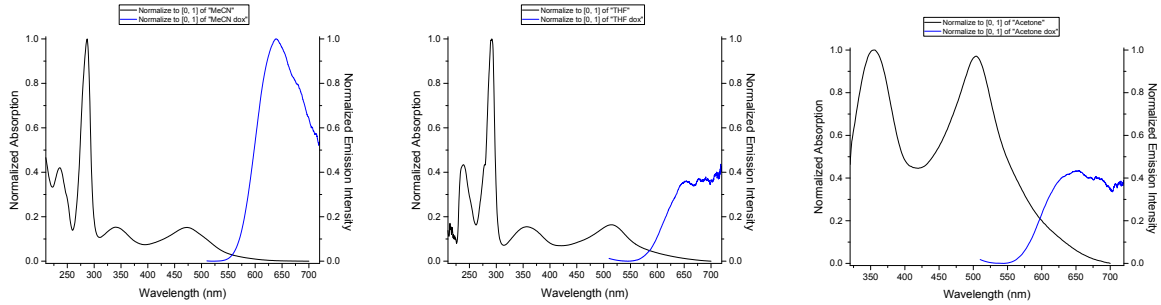

1c	**Absorption** λ nm (ε x 10^{-3} $M^{-1}cm^{-1}$)	**Emission** λ nm (% decrease)
MeCN	236 (23474), 287 (55804), 341 (8562), 473 (8502)	640 (58%)
THF	239 (30312), 292 (69465), 357 (10999), 515 (11610)	655 (57%)
Acetone	355 (9621), 505 (9348)	651 (48%)

2a:

(included in main manuscript)

2a	**Absorption** λ nm (ε x 10^{-3} $M^{-1}cm^{-1}$)	**Emission** λ nm (% decrease)
MeCN	237 (18326), 282 (43084), 339 (5355), 364 (5535), 444 (7066)	624 (23%)
THF	240 (17069), 288 (38912), 332 (5482), 453 (5637)	650 (26%)
Acetone	341 (6150), 363 (6217), 447 (7094)	630 (23%)

2b:

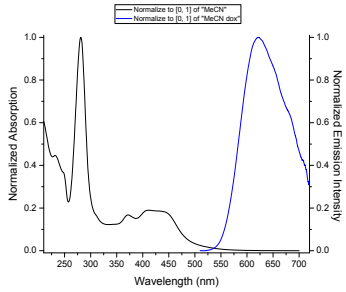

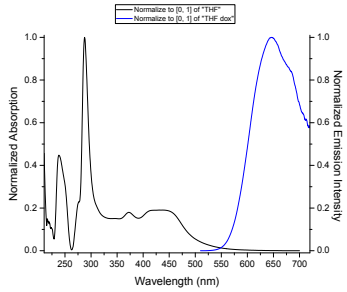

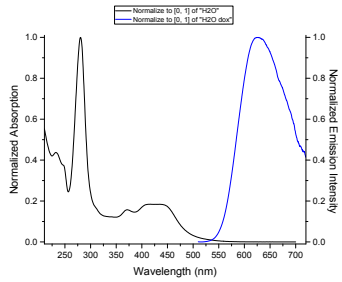

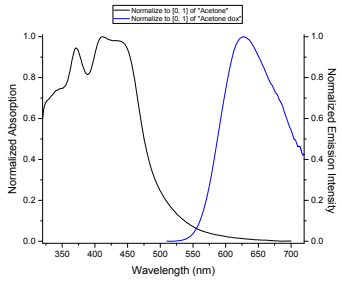

2b	**Absorption** λ nm (ε x 10^{-3} $M^{-1}cm^{-1}$)	**Emission** λ nm (% decrease)
MeCN	232 (21800), 281 (48944), 333 (5925), 373 (8119), 411 (9208), 429 (9044)	621 (20%)
THF	239 (21578), 288 (48234), 345 (7269), 373 (8655), 422 (9145), 438 (9176)	646 (28%)
H_2O	233 (21596), 281 (49385), 372 (7769), 416 (9104), 435 (9091)	625 (9%)
Acetone	372 (8832), 412 (9350), 433 (9171)	626 (27%)

2c:

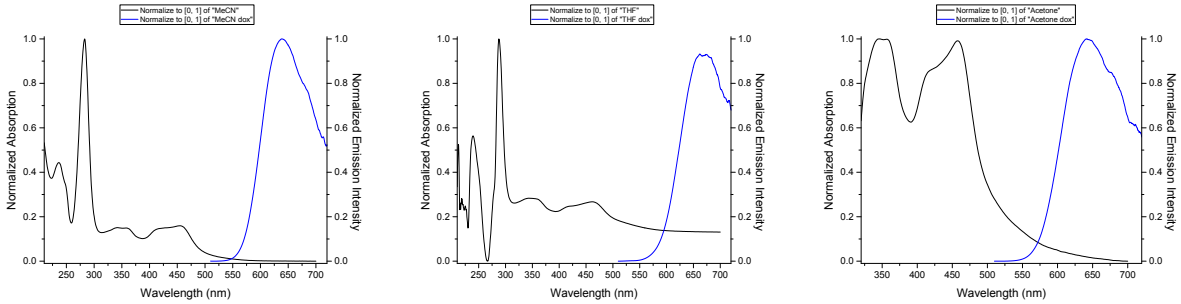

2c	**Absorption** λ nm (ε x 10^{-3} $M^{-1}cm^{-1}$)	**Emission** λ nm (% decrease)
MeCN	236 (19390), 283 (43887), 342 (6523), 358 (6445), 455 (6892)	638 (53%)
THF	240 (21144), 288 (42437), 343 (7440), 462 (6647)	662 (55%)
Acetone	347 (7356), 458 (7292)	642 (4%)

Figure S23. Above: Normalized UV/vis absorption (black) and emission (blue, λ_{ex} = 420 nm) spectra at 298 K, in deaerated solvents in optically dilute solutions. Below: Absorption and emission (emission intensity decrease = $100 \cdot I_{non\text{-}deaerated}/I_{aerated}$) data at 298 K, in different solvents.

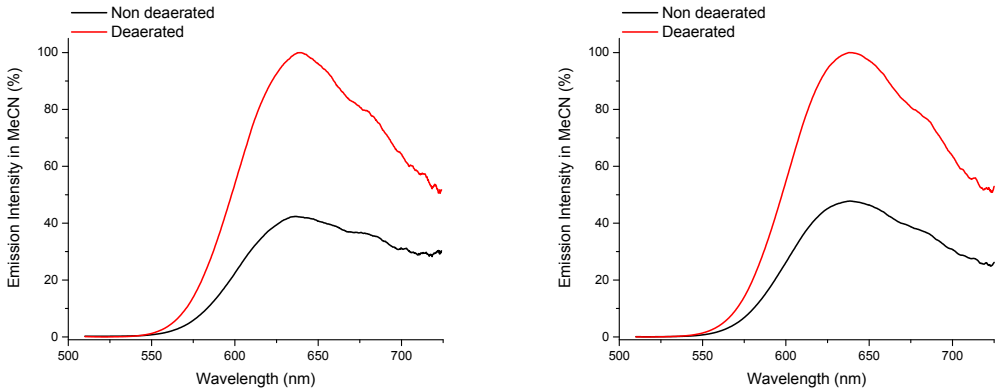

Figure S24. Emission spectra of **1c** (left) and **2c** (right) in aerated (black) and deaerated (red) MeCN.

3. Photocatalytic experiments

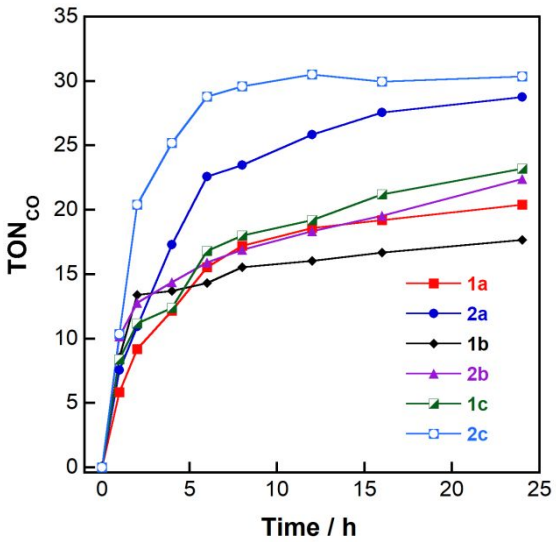

Figure S25. Turnover number of CO (TON_{CO}) evolved from 0.1 mM **Ru** complexes, 1.6 mM $[Ru(bpy)_3]^{2+}$ in a CO_2-saturated CH_3CN-TEOA solution (5:1 v/v) irradiated by >300 nm visible light.

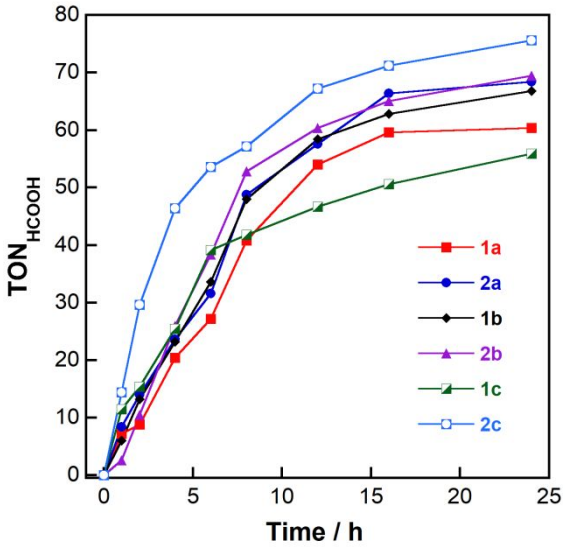

Figure S26. Turnover number of HCO_2^- (TON_{HCO2-}) evolved from 0.1 mM **Ru** complexes, 1.6 mM $[Ru(bpy)_3]^{2+}$ in a CO_2-saturated CH_3CN-TEOA solution (5:1 v/v) irradiated by >300 nm visible light.

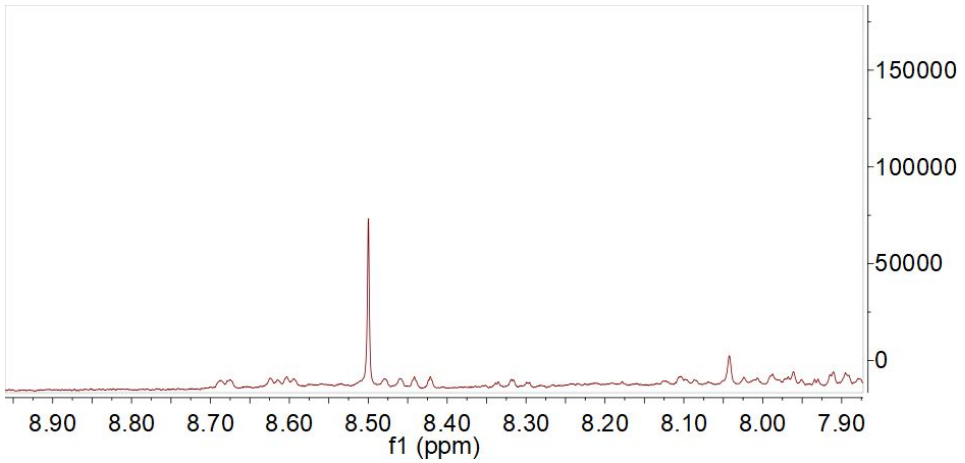

Figure S27. ^{1}H NMR spectrum of the photochemical solution of 1c indicating the formate chemical shift (δ = ~8.50 ppm) after workup involving addition of known amounts of Verkade's base and ferrocene (as an internal standard).